



HAL
open science

Full Band Monte Carlo simulation of phonon transfer at interfaces

N.D. Le, B. Davier, P. Dollfus, Marco G. Pala, A. Bournel, J. Saint-Martin

► **To cite this version:**

N.D. Le, B. Davier, P. Dollfus, Marco G. Pala, A. Bournel, et al.. Full Band Monte Carlo simulation of phonon transfer at interfaces. 2020 International Conference on Simulation of Semiconductor Processes and Devices (SISPAD), Sep 2020, Kobe, Japan. pp.27-30, 10.23919/SISPAD49475.2020.9241629 . hal-03029928

HAL Id: hal-03029928

<https://hal.science/hal-03029928>

Submitted on 17 Dec 2020

HAL is a multi-disciplinary open access archive for the deposit and dissemination of scientific research documents, whether they are published or not. The documents may come from teaching and research institutions in France or abroad, or from public or private research centers.

L'archive ouverte pluridisciplinaire **HAL**, est destinée au dépôt et à la diffusion de documents scientifiques de niveau recherche, publiés ou non, émanant des établissements d'enseignement et de recherche français ou étrangers, des laboratoires publics ou privés.

Full Band Monte Carlo simulation of phonon transfer at interfaces

N. D. Le¹, B. Davier^{1,2}, P. Dollfus¹, M. Pala¹, A. Bournel¹, J. Saint-Martin¹

¹Université Paris-Saclay, CNRS, Centre de Nanosciences et de Nanotechnologies, 91120, Palaiseau, France

²Department of Mechanical Engineering, The University of Tokyo, Tokyo 113-856, Japan

Abstract: Our home made Full-Band particle Monte Carlo is used to investigate the thermal interface conductance at Silicon/Germanium heterojunctions.

1. Introduction

As self-heating effect could degrade electronic device performances [1], understanding the nature of heat transport at the nanoscale is important for the CMOS industry [2]. In particular, the contribution of out-of-equilibrium phonons in heat transfer at interfaces remains an important issue.

Molecular Dynamics (MD) [3,4] and Non Equilibrium Green's function (NEGF) [5,6] simulations have been used to investigate this topics. The method of MD, provided important results to the study of heat transport as the complex structures of interfaces can be described at the atomic level in terms of roughness, strain and anharmonic phonon/phonon scattering mechanisms [7–9]. However, the size of the system that can be studied is limited to few thousands of atoms. Whereas MD only takes into account the classical nature of phonon transport, NEGF, by contrast, considers its quantum nature as interference and Bose-Einstein statistics can be captured. It is a very efficient method to calculate the transmission coefficient through interface, but is preferred for small and low-dimensional systems rather than micrometer long systems [10–13].

The particle Monte Carlo (MC) algorithm [14–16] is a powerful and complementary tool to investigate the heat transfer as the simulated system size can vary from the nanoscale to the microscale. MC solves the Boltzmann Transport Equation (BTE) for phonons without any assumption on the distribution function, thus the out-of-equilibrium transport regime is naturally taken into account. Besides, with convenient modeling, particle scattering mechanisms can be accurately described in the full phase space especially at the interfaces.

In this work, our Full-Band (FB) particle Monte Carlo [17] approach has been extended to treat the phonon transport at semi-transparent interfaces and used to extract and analyze the thermal interface conductance at Silicon/Germanium heterojunctions.

2. Full Band Monte Carlo

In the particle Monte Carlo method dedicated to

phonon transport, the trajectories of a large number of phonons are randomly selected according to relevant scattering rates and phonon dispersion that is in our case a Full-Band description. “Full Band Monte Carlo” means that all the phonon states in the first 3D Brillouin zone are considered as detailed in Ref. [17]. Here, the phonon dispersion, phonon velocity in cubic Si and cubic Ge have been calculated by using the Adiabatic Bond Charge Model (ABCM) [18] and employed as an input for the Monte Carlo simulations. The first Brillouin zone was discretized into a sampling of 29791 (31×31×31) wave vectors.

For Silicon, the phonon scattering rates have been derived from DFT as presented in Ref. [19]. For Germanium which is a heavier atom, DFT approach is more complex. Consequently a set of Holland parameters specific to a FB approach [20] has been adjusted to fit the bulk thermal conductivity in the full temperature range. The considered relaxation times are those of the three-phonon scattering and phonon-impurity scattering processes.

According to the definition used in Ref. [21], three out-of-equilibrium temperatures T , T^+ and T^- are defined. The pseudo temperature T is the temperature of an equilibrium distribution of phonons having the same energy density considering the total population of phonon. T^+ and T^- are called “hemispherical temperatures” and are defined by considering only the phonons with positive or only those with negative velocity, respectively.

3. Semi-transparent interface modeling

When a particle collides with a semi-transparent interface, both elastic and diffusive mechanisms are considered. Besides, the probability of transmission of a phonon colliding the interface is obtained within the Full-Band Diffusive Mismatch Model (DMM) [22]. In this model, the interface is assumed to have many defects so that each phonon colliding the interface loses totally the memory of its initial state. The wave vector and the mode of the phonon in the final state are independent of those in the initial state. The only conserved quantity is the phonon energy. Thus, the transmission coefficient depends only on the phonon energy, and neither on the wave vector, nor on the state of the phonon.

As the reflection and transmission processes are

assumed to be diffusive and elastic, the angular distribution of the wave vector of reflected or transmitted phonon is chosen randomly over the states belonging to the same isoenergy surface to satisfy the energy conservation. Moreover, the appearance of a net flux along the interface must be prohibited and a Full-Band version of the Lambert's emission law [23] must be applied to avoid a non-physical accumulation of phonons near the interface. Thus, among the states belonging to the same isoenergy surface, the final state j and thus the final wave vector \vec{q}_j (and mode) are selected according to this following statistic weight:

$$P_j \propto \vec{v}_j \cdot \vec{n} \quad (1)$$

where \vec{v}_j is the group velocity of the state j and \vec{n} is the vector normal to the interface.

4. Simulated Devices

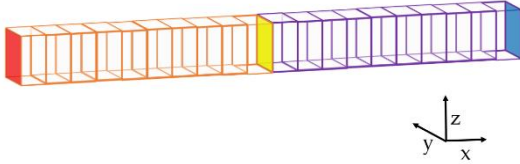


Fig. 1. Si/Ge heterostructure. Orange and violet cells are made of Si and Ge, respectively. Hot and cold thermostats are in red and blue, respectively. DMM interface is in Yellow. White faces stand for periodic boundaries.

Fig. 1 shows the simulated Si/Ge heterostructure of length L . One device end is in contact with a hot thermostat at temperature T_H and the other end is in contact with a cold thermostat at temperature T_C . The Si/Ge junction is located at the middle of the device ($x = L/2$). The interface between Si and Ge is assumed to be abrupt. The width w and height h of the heterostructure (along y and z directions, respectively) are equal to 100 nm. As the cross-plane transport configuration is simulated, the structures are supposed to be infinite along the y and z directions. In that purpose, external interfaces that are normal to y and z directions follow periodic boundary conditions.

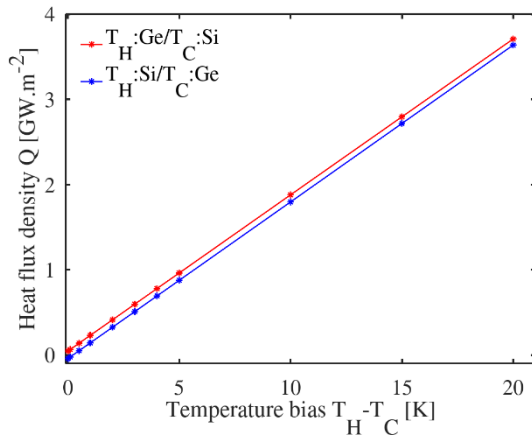


Fig. 2. Heat flux density in a Si/Ge heterostructure of length $L=20$ nm as a function of the applied temperature bias T_H-T_C .

$$(T_H+T_C)/2=300K.$$

The system is primarily uniformly meshed along the x -axis by using 20 cells. Then, this mesh could be refined at 5 nm around the heterojunction and near the thermostats to keep the cell length equal to or lower than 1 nm. It should be noticed that the size of a cell should be significantly higher than the atomic radii of Ge (125 pm) and Si (110 pm) [24] i.e. it should remain in the order of magnitude of nanometer.

5. Results

Fig. 2 shows the simulated heat flux density Q as a function of the temperature difference between the two thermostats for a 20 nm long Si/Ge heterostructure. For all studied temperature biases, the cold and hot thermostats have been swapped. The evolution of the flux is clearly a linear function of the temperature difference. The linear coefficient gives a total thermal conductance of the heterostructure (for both thermostat configurations) of $G_{tot} = 183$ MW/m²/K.

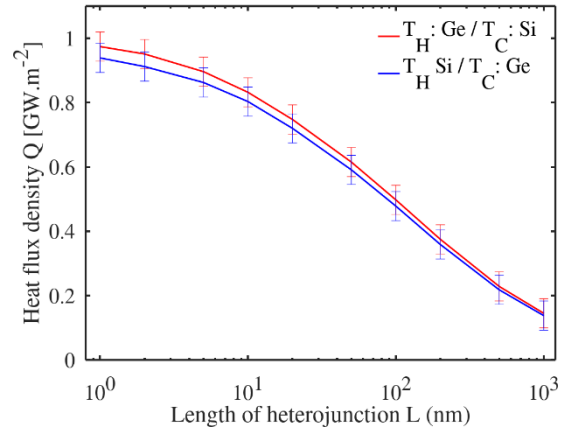


Fig. 3. Heat flux density in a Si/Ge heterostructure as a function of the device length L . $T_H=302$ K and $T_C=298$ K.

However for $T_H - T_C = 0$ K, a non-zero flux of $\delta Q = 45.3$ MW/m² is extracted from the simulation. This value is assumed to be a good estimate of the MC simulation resolution. The statistical error for the calculation of a physical quantity f by using the Monte Carlo method is [25]:

$$|f - \langle f \rangle| < \alpha \sqrt{\frac{\langle f^2 \rangle - \langle f \rangle^2}{N}}, \quad (2)$$

where N is the number of random observations of the quantity f . Assuming that f follows the normal distribution, the interval of 95% confidence corresponds to $\alpha = 1.96$. By increasing N , the statistical error can be reduced as needed. Nevertheless, the resolution of our MC simulation is the lower limit of the error related to the heat flux density estimation and will be used in the following to define the error bars.

In Fig. 3, the heat flux density Q is plotted as a function of the device length L for a temperature bias

$T_H - T_C$ of 4.0 K. In ultra-short devices ($L < 100$ nm), the fluxes tend to saturate and to become independent of the length as the phonon transport becomes ballistic. In long devices ($L > 100$ nm) in which the transport is diffusive, the heat flux density tends to decrease linearly when L increases. Moreover, the thermostat swap induces a shift of the flux smaller than the error bar of the MC simulation, thus no significant thermal rectification can be observed.

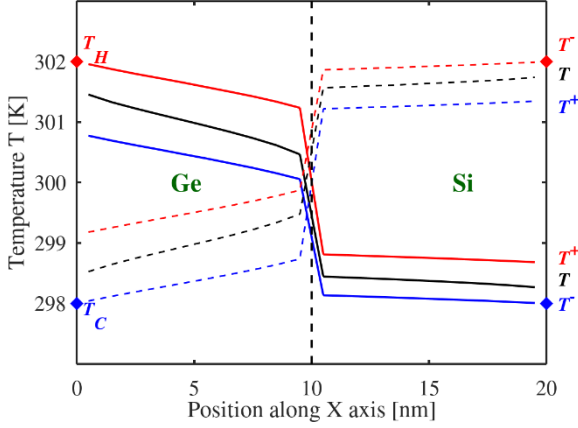


Fig. 4. Temperature profiles in a Si/Ge heterostructure of length $L=20$ nm in contact with $T_H = 302$ K (298 K), $T_C = 298$ K (302 K) in continuous lines (in dashed lines, respectively).

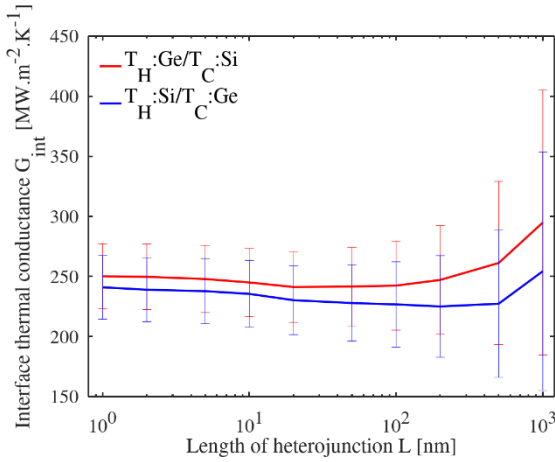


Fig. 5. Thermal interface conductance in a Si/Ge heterostructure as a function of the device length L at 300 K and with a temperature bias of $T_H - T_C = 4$ K

Fig. 4 presents the temperature profiles: T , T^+ and T^- in a 20 nm long device for both positive and negative temperature biases of 4 K. In the first configuration, the Ge bar is in contact with the hot thermostat and the Si bar is in contact with the cold thermostat (solid line) and, as the flux is positive along the x axis, T^+ is the highest temperature. By swapping the heterostructure bias (dashed line), the thermal flux is reversed and the phonons having positive x -velocity, i.e. propagating from the cold to the hot thermostat, are minority. Thus, in this

configuration T^+ is the lowest temperature.

The temperature drop at the interface is sharp while the temperature gradient in the Si and Ge bars are weak. Besides, all the temperatures gradients (of T , T^+ and T^-) are higher in Ge than in Si as Ge exhibits lower thermal conductivity. Moreover, the gradient of T is slightly higher than those of T^+ and T^- . It should be noted that, the net thermal flux is governed by the gradient of T within the Fourier's formalism or the difference between T^+ and T^- at a given position within the formalism of Ref. [21].

The interface thermal conductance is finally computed from dividing the heat flux density Q by the difference of the hemispherical temperatures T^+ and T^- on each side of the interface [21]:

$$G_{int} = \frac{Q}{T^+(L/2 - \delta x) - T^-(L/2 + \delta x)} \quad (3)$$

where δx stands for an infinitely small distance.

From the previous results of the resolution of the heat flux density and the total thermal conductance, the resolution of the temperature bias is estimated by using the following ratio:

$$\delta(\Delta T) = \frac{\delta Q}{G_{tot}} = 0.25 \text{ K} \quad (2)$$

For the device of length L , the lower bound for the statistical error of the interface thermal conductance $\delta G_{int}(L)$ is deduced from the resolutions of the heat flux density and the temperature bias according to:

$$\frac{\delta G_{int}(L)}{G_{int}(L)} = \frac{\delta Q(L)}{Q(L)} + \frac{\delta(\Delta T)}{T_H - T_C} \quad (3)$$

The resulting G_{int} are plotted in Fig. 5 for several device lengths. The width of error bar increases when the length L increases as the temperature difference ($T_H - T_C$) near the interface also decreases leading to higher uncertainty in terms of extracted temperature.

However, the variation of G_{int} as a function of the device length remains lower than the error bars. Thus, G_{int} appears to be equal to 243.3 ± 41.9 MW/m² independently of the device length. This is consistent with the DMM theory which predicts a unique value for the Si/Ge interface conductance of 225 MW/m²/K [22]. The modification of the transport regime of phonon in the studied length range does not affect G_{int} .

It should be noticed that the standard definition of the interface thermal conductance $G_{int}^T = Q/[T(L/2 - \delta x) - T(L/2 + \delta x)]$ using only the pseudo temperature T leads to different results. Indeed, the values of G_{int}^T that are 360 MW/m² for $L=1$ nm and 350 MW/m² for $L=100$ nm. are significantly higher than the DMM results.

Ensuring by assumptions spectral energy balance, the DMM does not provide by itself any physical ingredient that could induced thermal rectification. However, the presence of out of equilibrium phonons could have generated such asymmetry in the phonon transport. In Fig. 5, the difference between the values of G_{int} when heat

flux is reversed is still smaller than the error bars and no thermal rectification due to “hot” phonons is observed.

6. Conclusion

In this work, the heat transfer through Si/Ge interfaces was investigated by using Full Band Monte Carlo simulation for phonon using DMM for modeling the phonon transmission at semi-transparent interfaces. Our MC simulator is able to calculate all the relevant temperature profiles, the heat flux density and finally the interface thermal conductance at heterojunctions. It can simulate short systems working in ballistic regime as well as long devices working in diffuse transport regime.

A linear relationship was obtained between the heat flux density and the applied temperature difference across a short heterostructure of 20 nm. Thus, even in the case of a strongly ballistic phonon transport, the concept of thermal conductance remains relevant. Moreover, the value of the interface thermal conductance obtained from this MC approach are consistent with the semi-analytical DMM model by using the concept of hemispherical temperature T^+ and T^- . Besides, no thermal rectification is observed in our model at the Si/Ge interface.

Finally, this work demonstrates the relevance of this MC simulator to investigate the heat transport at the nanoscale as it provides very detailed insight into thermal transfer at interfaces.

References

- [1] T. Thu Trang Nghiê, J. Saint-Martin, and P. Dollfus, *Journal of Applied Physics* **116**, 074514 (2014).
- [2] C. Prasad, *IEEE Transactions on Electron Devices* **66**, 4546 (2019).
- [3] S. Merabia and K. Termentzidis, *Physical Review B - Condensed Matter and Materials Physics* **86**, 094303 (2012).
- [4] E. S. Landry and A. J. H. McGaughey, *Physical Review B - Condensed Matter and Materials Physics* **80**, 165304 (2009).
- [5] N. Mingo, *Physical Review B - Condensed Matter and Materials Physics* **74**, 125402 (2006).
- [6] S. Sadasivam, U. V. Waghmare, and T. S. Fisher, *Physical Review B* **96**, 174302 (2017).
- [7] P. Chantrenne and J. L. Barrat, *Journal of Heat Transfer* **126**, 577 (2004).
- [8] R. Rurali, X. Cartoixà, and L. Colombo, *Physical Review B - Condensed Matter and Materials Physics* **90**, 041408 (2014).
- [9] K. R. Hahn, M. Puligheddu, and L. Colombo, *Physical Review B - Condensed Matter and Materials Physics* **91**, 195313 (2015).
- [10] N. Mingo and L. Yang, *Physical Review B - Condensed Matter and Materials Physics* **68**, 245406 (2003).
- [11] N. Mingo and L. Yang, *Physical Review B - Condensed Matter and Materials Physics* **70**, 249901(E) (2004).
- [12] W. Zhang, T. S. Fisher, and N. Mingo, *Journal of Heat Transfer* **129**, 483 (2007).
- [13] C. Monachon, L. Weber, and C. Dames, *Annual Review of Materials Research* **46**, 433 (2016).
- [14] S. Mazumder and A. Majumdar, *Journal of Heat Transfer* **123**, 749 (2001).
- [15] D. Lacroix, K. Joulain, and D. Lemonnier, *Physical Review B - Condensed Matter and Materials Physics* **72**, 064305 (2005).
- [16] J. P. M. Péraud and N. G. Hadjiconstantinou, *Physical Review B - Condensed Matter and Materials Physics* **84**, 205531 (2011).
- [17] B. Davier, J. Larroque, P. Dollfus, L. Chaput, S. Volz, D. Lacroix, and J. Saint-Martin, *Journal of Physics Condensed Matter* **30**, 495902 (2018).
- [18] W. Weber, *Physical Review B* **15**, 4789 (1977).
- [19] L. Chaput, J. Larroque, P. Dollfus, J. Saint-Martin, and D. Lacroix, *Appl. Phys. Lett.* **112**, 033104 (2018).
- [20] M. G. Holland, *Physical Review* **132**, 2461 (1963).
- [21] B. Davier, P. Dollfus, S. Volz, J. Shiomi, U. Paris-saclay, C. De Nanosciences, and D. Nanotechnologies, *ArXiv* (2020).
- [22] J. Larroque, P. Dollfus, and J. Saint-Martin, *Journal of Applied Physics* **123**, 025702 (2018).
- [23] W. J. Smith, *The Design of Optical Systems: General*, 4th ed. (McGrawHill, 2008).
- [24] J. C. Slater, *The Journal of Chemical Physics* **41**, 3199 (1964).
- [25] S. Volz, R. Carminati, P. Chantrenne, S. Dilhaire, S. Gomez, N. Trannoy, and G. Tessier, *Microscale and Nanoscale Heat Transfer* (Springer, 2007).